

AperTO - Archivio Istituzionale Open Access dell'Università di Torino

**Cancer-associated fibroblasts promote aggressive gastric cancer phenotypes via heat shock factor 1-mediated secretion of extracellular vesicles**

**This is the author's manuscript**

*Original Citation:*

*Availability:*

This version is available <http://hdl.handle.net/2318/1797873> since 2021-08-24T14:52:47Z

*Published version:*

DOI:10.1158/0008-5472.CAN-20-2756

*Terms of use:*

Open Access

Anyone can freely access the full text of works made available as "Open Access". Works made available under a Creative Commons license can be used according to the terms and conditions of said license. Use of all other works requires consent of the right holder (author or publisher) if not exempted from copyright protection by the applicable law.

(Article begins on next page)

**Cancer-Associated Fibroblasts Promote Aggressive Gastric Cancer Phenotypes Via Heat Shock Factor 1-Mediated Secretion of Extracellular Vesicles**



Nil Grunberg<sup>1</sup>, Meirav Pevsner-Fischer<sup>1</sup>, Tal Goshen-Lago<sup>2</sup>, Judith Diment<sup>3</sup>, Yaniv Stein<sup>1</sup>, Hagar Lavon<sup>1</sup>, Shimrit Mayer<sup>1</sup>, Oshrat Levi-Galibov<sup>1</sup>, Gil Friedman<sup>1</sup>, Yifat Ofir-Birin<sup>1</sup>, Li-Jyun Syu<sup>4</sup>, Cristina Migliore<sup>5</sup>, Eyal Shimoni<sup>6</sup>, Salomon M. Stemmer<sup>7,8</sup>, Baruch Brenner<sup>7,8</sup>, Andrzej A. Dlugosz<sup>4,9</sup>, David Lyden<sup>10</sup>, Neta Regev-Rudzki<sup>1</sup>, Irit Ben-Aharon<sup>2,11</sup>, and Ruth Scherz-Shouval<sup>1</sup>

**ABSTRACT**

Gastric cancer is the third most lethal cancer worldwide, and evaluation of the genomic status of gastric cancer cells has not translated into effective prognostic or therapeutic strategies. We therefore hypothesize that outcomes may depend on the tumor microenvironment (TME), in particular, cancer-associated fibroblasts (CAF). However, very little is known about the role of CAFs in gastric cancer. To address this, we mapped the transcriptional landscape of human gastric cancer stroma by microdissection and RNA sequencing of CAFs from patients with gastric cancer. A stromal gene signature was associated with poor disease outcome, and the transcription factor heat shock factor 1 (HSF1) regulated the signature. HSF1

upregulated inhibin subunit beta A and thrombospondin 2, which were secreted in CAF-derived extracellular vesicles to the TME to promote cancer. Together, our work provides the first transcriptional map of human gastric cancer stroma and highlights HSF1 and its transcriptional targets as potential diagnostic and therapeutic targets in the genomically stable tumor microenvironment.

**Significance:** This study shows how HSF1 regulates a stromal transcriptional program associated with aggressive gastric cancer and identifies multiple proteins within this program as candidates for therapeutic intervention.

**Introduction**

Gastric cancer is the fifth most common cancer and the third most lethal cancer, worldwide (1). Recent advances in treatment were made possible due to better classification of gastric cancer subtypes, but the prognosis of advanced gastric cancer remains poor and many patients get diagnosed at an advanced stage of the disease due to limited understanding of the underlying biology (2). There is an urgent need to

better understand the molecular basis of this disease, and to identify biomarkers that may predict outcome and guide therapy.

Gastric cancer is a heterogeneous disease. Traditionally, anatomical location (true gastric vs. gastro-esophageal) and histologic characteristics (diffuse vs. intestinal; tubular vs. papillary) have been used to classify gastric cancer subtypes (2). Recent advances in molecular understanding have enabled classification of gastric cancer into different subtypes based on chromosomal instability, microsatellite instability, genomic stability, presence of Epstein-Barr virus, and epithelial-mesenchymal transition (EMT), which were associated with different survival outcomes (3–6). Mutations in *CDH1* and *KRAS*, and overexpression of *HER2*, *EGFR*, *FGFR2*, *VEGF*, were shown to contribute to disease progression and correlate with poor outcome (7, 8). Despite serving as valuable guides in deciphering the complexity of gastric cancer, there has been little success in applying these molecular classifiers to treatment stratification and development of targeted therapies (3). Prognosis in the clinic is still mostly evaluated on the basis of TNM staging (tumor size, lymph node involvement, and metastasis), and the standard of care for localized gastric cancer is surgical intervention combined with chemotherapy (7).

Increasing evidence over the past decade highlighted the indispensable contribution of the tumor microenvironment (TME) to disease progression and treatment resistance (9). The TME is comprised of various cell types, including endothelial cells, fibroblasts, macrophages, and lymphocytes, as well as extracellular matrix components (ECM; ref. 10). The immune microenvironment of gastric cancer has gained increasing attention over the last years, due to its potential effect on immunotherapy in patients with high microsatellite instability (11). Yet little is known about the contribution of cancer-associated fibroblasts (CAF) to gastric cancer progression and metastasis. CAFs are the most abundant cell type in a variety of carcinomas (12). They support cancer cells by modifying the ECM, promoting angiogenesis, and maintaining a chronic inflammatory state (12–17). In gastric cancer,

<sup>1</sup>Department of Biomolecular Sciences, The Weizmann Institute of Science, Rehovot, Israel. <sup>2</sup>Division of Oncology, Rambam Health Care Campus, Haifa, Israel. <sup>3</sup>Department of Pathology, Kaplan Medical Center, Rehovot, Israel. <sup>4</sup>Department of Dermatology, Rogel Cancer Center, University of Michigan, Ann Arbor, Michigan. <sup>5</sup>University of Torino, Department of Oncology, Candiolo; Candiolo Cancer Institute, FPO-IRCCS, Candiolo, Italy. <sup>6</sup>Department of Chemical Research Support, The Weizmann Institute of Science, Rehovot, Israel. <sup>7</sup>Institute of Oncology, Davidoff Cancer Center, Rabin Medical Center, Beilinson Hospital, Petah Tikva, Israel. <sup>8</sup>Sackler Faculty of Medicine, Tel Aviv University, Ramat Aviv, Tel Aviv, Israel. <sup>9</sup>Department of Cell & Developmental Biology, Rogel Cancer Center, University of Michigan, Ann Arbor, Michigan. <sup>10</sup>Children’s Cancer and Blood Foundation Laboratories, Departments of Pediatrics, and Cell and Developmental Biology, Drukier Institute for Children’s Health, Meyer Cancer Center, Weill Cornell Medicine, New York, New York. <sup>11</sup>Rappaport Faculty of Medicine, Technion, Haifa, Israel.

**Note:** Supplementary data for this article are available at Cancer Research Online (<http://cancerres.aacrjournals.org/>).

**Corresponding Author:** Ruth Scherz-Shouval, Department of Biomolecular Sciences, Weizmann Institute of Science, Ullmann Building 237, Rehovot, 76100, Israel. E-mail: [ruth.shouval@weizmann.ac.il](mailto:ruth.shouval@weizmann.ac.il)

Cancer Res 2021;XX:XX-XX

doi: 10.1158/0008-5472.CAN-20-2756

©2021 American Association for Cancer Research.

82	accumulation of CAFs is correlated with increased tumor size, invasion, and metastasis (18). Recently, the abundance of natural killer cells, endothelial cells, and CAFs was shown to predict chemotherapy benefit in gastric cancer (19). However, the specific genes and molecular events contributing to these protumorigenic effects are not well understood. To address this, we set out to map the transcriptional landscape of gastric CAFs. Using laser-capture microdissection (LCM) and RNA-sequencing (RNA-seq) of CAFs from patients with gastric cancer, we define a gene-signature associated with poor disease outcome. We characterize this signature using mouse models and co-culture assays, and show that components of this signature are regulated by the master transcriptional regulator heat shock factor 1 (HSF1; ref. 20), and secreted from CAFs via extracellular vesicles (EV). These fibroblast-derived EVs contribute to tumor growth in an HSF1-dependent manner. Together, our work provides a comprehensive map of gastric cancer stromal transcription with potential implications on prognosis and treatment.	140
83		141
84		142
85		143
86		144
87		145
88		146
89		147
90		148
91		149
92		150
93		151
94		152
95		153
96		154
97		155
98		
	<b>Materials and Methods</b>	
99		
100	<b>Ethics statement</b>	
101	Clinical samples and patient data were collected following approval by the Rabin medical center Institutional Review Board (IRB, protocol no. 0297-11-RMC) with full exemption for consent form for anonymized samples. Human samples used for MxIF staining were obtained from the Israel National Biobank for Research (MIDGAM; <a href="https://www.midgam.org.il/">https://www.midgam.org.il/</a> ) under IRB no. 6141-19-SMC. These samples were collected from patients who provided written informed consent for collection, storage, distribution of samples, and data for use in future research studies. All animal studies were approved by the Institutional Animal Care and Use Committee (IACUC protocol nos. 15310619-2, 15140619-3, 06690820-3).	
102		
103		
104		
105		
106		
107		
108		
109		
110		
111		
112	<b>Mice</b>	
113	Athymic nude mice were purchased from Harlan Biotech. These mice, the triple-transgenic <i>Lgr5-EGFP-IRES-CreERT2; R26-LSL-rtTA-IRES-EGFP; tetO-GLI2A</i> mice (iLgr5;GLI2A mice; ref. 21), <i>Hsf1</i> null mice, and their WT littermates (BALB/c × 129SvEV, by Ivor J. Benjamin; ref. 22) were maintained under specific-pathogen-free conditions at the Weizmann Institute's animal facility.	
114		
115		
116		
117		
118		
119	<b>Cell lines and primary cell cultures</b>	
120	N87 gastric cancer cells were kindly provided by Yosef Yarden (WIS; originally from ATCC). N87 cells were transduced with GFP using a third-generation lentiviral system. MC38 colon cancer cells were kindly provided by Lea Eisenbach (WIS; originally from NCI). MC38 cells were transduced with mcherry-luciferase using a second-generation lentiviral system. Primary MEFs were produced from WT and <i>Hsf1</i> null mice. HFF cells were purchased from ATCC. MEFs, MC38 cells, and N87 cells were cultured in RPMI (#01-100-1A, Biological Industries) supplemented with 10% FBS (Invitrogen) and P/S (Biological Industries). HFF cells were cultured in DMEM (#01-052-1A, Biological Industries) supplemented with 15% FBS, 1.5% L-glutamine, and P/S. Cell lines were tested routinely for <i>Mycoplasma</i> using EZ-PCR Mycoplasma Test Kit (#20-700-20, Biological Industries). MEFs were used in passage 1. Other cell lines were maintained below passage 25.	
121		
122		
123		
124		
125		
126		
127		
128		
129		
130		
131		
132		
133		
134		
135	<b>Laser capture microdissection of human gastric cancer samples</b>	
136	LCM cohort patients were selected on the basis of patient outcome data (Supplementary Table S1). Stromal and cancer regions were marked by a trained pathologist blinded to clinical and outcome data	
137		
138		
	to include >90% CAFs for stroma and >90% cancer cells for cancer. Gastric muscle, immune islands, and blood vessels were excluded from microdissection. FFPE slides were deparaffinized and stained using Arcturus Paradise Plus Staining Kit (#KIT0312J; Thermo Fisher Scientific) according to the instructions of the manufacturer. Slides were left to dry for 5 minutes at RT followed by microdissection using the Arcturus (XT) laser microdissection instrument (#010013097, Thermo Fisher Scientific). Infrared capture was used to minimize RNA damage. CapSure Macro LCM caps (#LCM0211, Thermo Fisher Scientific) were used to capture microdissected tissue. To obtain sufficient material from these highly degraded RNA samples, we performed microdissection from 6 to 10, 5 μm sections per sample. Microdissected tissue from each sample was pooled together, and kept on dry ice until RNA isolation using the RNeasy FFPE Kit (#73504, Qiagen) with one modification—proteinase K digestion at 56°C was carried out for 1 hour.	140
		141
		142
		143
		144
		145
		146
		147
		148
		149
		150
		151
		152
		153
		154
		155
	<b>Library preparation, RNA-seq, and analysis of LCM samples</b>	
	Libraries were prepared using the SMARTer Stranded Total RNA-Seq v2-Pico Input Mammalian Kit (#634415, Takara Bio USA) according to the instructions of the manufacturer. Libraries were sequenced on Illumina NextSeq 500, at 50M reads for stroma and 25M reads for cancer samples, to provide sufficient reads to pass quality control filters of RNA-seq. Principal component analysis (PCA) was performed on full RNA-seq datasets for each sample (for stroma and cancer samples, separately). After calculating the first three main PCs (PCA1–3), we used the Robust Mahalanobis distance function to exclude potential outlier samples (see GitHub <a href="https://github.com/privetfl/bigutilr">https://github.com/privetfl/bigutilr</a> , and refs. 23–25). These robust Mahalanobis distances are approximately Chi-square distributed, which enables deriving <i>P</i> values of outliers (Supplementary Table S2). Because we used three dimensions, we chose a <i>P</i> value threshold of 0.00111 ( <i>P</i> value <0.01 with Bonferroni correction for multiple comparisons), which concluded that patient 5 is an outlier in PCA2 and PCA3. This patient was removed from all downstream analysis. Read counts of the 8 patients were normalized and tested for difference using DESeq2 (26). Hierarchical clustering was carried out using Pearson correlation with complete linkage and on differentially expressed genes (DEG), which were filtered with the following parameters: baseMean > 5, <i>P</i> <sub>adj</sub> < 0.1 and  logfoldchange  > 1. Pathway analysis was performed using Metascape, significant pathways were determined if <i>P</i> < 0.05 and FDR < 0.5. STRING analysis was performed including all DEGs.	156
		157
		158
		159
		160
		161
		162
		163
		164
		165
		166
		167
		168
		169
		170
		171
		172
		173
		174
		175
		176
		177
		178
		179
		180
		181
		182
	<b>CAF isolation and RNA-seq from iLgr5;GLI2A mice</b>	
	Gastric cancer was induced in iLgr5;GLI2A mice as described in ref. 21. Gastric tumors were harvested post mortem, washed, minced, and dissociated using a gentleMACS dissociator and enzymatic digestion with DMEM containing 3 mg/mL collagenase A (#11088793001, Sigma Aldrich) and 0.1 mg/mL Deoxyribonuclease I (#LS002007, Worthington) for 20 minutes at 37°C. The single cell suspension was washed, filtered using 100 μm cell strainer, and immunostained. Normal gastric fibroblasts or CAFs were collected on the basis of negative selection for ghost dye, CD45, EpCAM, and CD31 and positive selection for PDPN. RNA-seq was done by MARS-Seq as described in ref. 27. DEGs were filtered with the following parameters: baseMean > 5, <i>P</i> <sub>adj</sub> < 0.01, and  logfoldchange  > 3. Pathway analysis was performed using Metascape, significant pathways were determined if <i>P</i> < 0.05 and FDR < 0.5.	183
		184
		185
		186
		187
		188
		189
		190
		191
		192
		193
		194
		195
		196
		197
		198

201	<b>Validation of the patient and iLgr5;GLI2A mouse stromal signatures in independent patient cohorts</b>	260
202		261
203	Patient data from the TCGA, Singapore (GSE15460), KUGH_	
204	KUCM (GSE26942), and ACRG cohorts (GSE62254) were down-	
205	loaded, individual gene values were transformed to z-scores and the	
206	average of all known genes per sample was used to determine scores for the	
207	upregulated and downregulated signatures. For the <i>INHBA-</i>	
208	<i>THBS1-THBS2</i> gene-signature individual, gene values were trans-	
209	formed to z-scores and the average of genes per sample was deter-	
210	mined. Gene symbols were matched through Affymetrix Human	
211	Genome U133 Plus 2.0 Array or Illumina HumanHT-12 V4.0 expres-	
212	sion bead chip. For patient cohorts GSE15460 and GSE62254, we could	
213	match 109 DEGs from the CAF_up_sig and CAF_down_sig; and for	
214	GSE26942, we could match 87 DEGs from the CAF_up_sig and	
215	CAF_down_sig (out of the total 129 DEGs). For the iLgr5;GLI2A	
216	mCAF_up_sig and mCAF_down_sig, 314 DEGs were matched in the	
217	GSE15460 and GSE62254 cohorts and 271 DEGs in the GSE26942	
218	cohort (out of the total 361 DEGs). Median signature was calculated	
219	using patients with complete survival and signature information.	
220	Kaplan–Meier (KM) analysis of overall survival with log rank <i>P</i> value	
221	was performed for each cancer type or patient cohort on patients	
222	stratified by median expression of each of these signatures.	
223	<b>HSF1 scoring and analysis</b>	
224	Nuclear HSF1 staining in stroma and cancer cells of 72 patients was	
225	analyzed by a trained pathologist who was blinded to both patient	
226	outcome and clinical data. A scale of 0 to 3 (0–3: low ≤ 1; 1.5 <	
227	intermediate ≤ 2; high >2) was set by the pathologist and scores were	
228	given on the basis of nuclear staining of HSF1 in stroma and cancer	
229	cells (Supplementary Table S1). Tissue samples were obtained from	
230	surgical specimens. Patients diagnosed as stage 1 to 3 did not present	
231	with metastases at diagnosis. Eight patients diagnosed as stage 4 gastric	
232	cancer with metastases were omitted from further analysis. Overall	
233	survival was defined as the time from first diagnosis to death based on	
234	the clinical data outlined in Supplementary Table S1. The scores in	
235	cancer cells and CAFs showed different distributions. Therefore, for	
236	survival analysis of HSF1 activation in cancer cells, patients with low	
237	and intermediate scores were combined and compared with patients	
238	with high scores, whereas for survival analysis of HSF1 activation in	
239	CAFs, patients with high and intermediate scores were combined and	
240	compared with patients with low scores (Supplementary Table S1).	
241	One patient could not be scored for cancer and for CAF HSF1 due to	
242	insufficient tumor tissue and was therefore excluded from all statistical	
243	analyses. Two patients could not be scored for CAF HSF1 and were	
244	excluded from CAF HSF1 analysis. Stage 2/3 was scored as stage 2 in	
245	the final clinical analysis.	
246	<b>Co-injection of recombinant activin A and THBS2 with MC38 cancer cells into nude mice</b>	
247		
248	MC38 ( $2 \times 10^5$ ) were incubated with either PBS, 2.5 μg of Activin A	
249	(#CYT-146, ProSpec), or 2.5 μg of THBS2 (#1635-T2, R&D Systems)	
250	and co-injected in a total volume of 100 μL subcutaneously into Nude	
251	mice (Harlan laboratories). Forty-eight hours later, a second dose of	
252	2.5 μg recombinant protein was injected. Tumors were measured by	
253	caliper for size and mice were sacrificed at day 15 due to high burden in	
254	the Activin A group.	
255	<b>Co-injection of EVs with MC38 cancer cells into nude mice</b>	
256	MC38 cells ( $2 \times 10^5$ ) were co-injected with either PBS or $1 \times 10^{10}$ WT	
257	or <i>Hsf1</i> null EVs subcutaneously into Nude mice (Harlan laboratories).	
258	Forty-eight hours later, a second dose ( $5 \times 10^9$ ) of EVs was injected.	
	Tumors were measured by caliper for size and the mice were sacrificed	260
	at day 17 due to high tumor burden.	261
	<b>Data availability statement</b>	262
	RNA-seq data of iLgr5;GLI2A mice and patient samples were	263
	deposited in Gene Expression Omnibus (GEO) and can be accessed	264
	via GSE162301 and GSE165211, respectively. All other data support-	265
	ing the findings of this study are available from the corresponding	266
	author on reasonable request.	267
	<b>Results</b>	268
	<b>CAFs express a transcriptional program that promotes malignancy and correlates with poor disease outcome in gastric cancer</b>	269
	Gastric CAFs have been attributed protumorigenic effects, however	270
	the genes contributing to these effects are largely unknown. Therefore,	271
	we mapped the transcriptome of gastric CAFs in the intratumoral	272
	stroma by laser capture microdissection (LCM) followed by RNA-seq	273
	(Supplementary Fig. S1A). We isolated and sequenced CAF-rich	274
	stromal regions from formalin-fixed paraffin-embedded (FFPE) tumor	275
	sections of 9 patients with gastric cancer (Supplementary Figs. S1B and	276
	S1C; Supplementary Table S1), representing favorable (survival) and	277
	poor prognostic (lethality) outcomes (Supplementary Table S3). PCA	278
	showed that stromal samples from these patients clustered on basis of	279
	disease outcome (Fig. 1A; Supplementary Fig. S1D), whereas cancer	280
	samples from the same patients did not (Fig. 1B; Supplementary	281
	Fig. S1E). Differential expression analysis of stromal samples (see	282
	Materials and Methods, Supplementary Table S2; Supplementary Figs.	283
	S1F and S1G) revealed 129 DEGs between favorable and poor outcome	284
	groups (Fig. 1C; Supplementary Table S3). ECM organization (involv-	285
	ing genes such as <i>AEBP1</i> , <i>COL10A1</i> , <i>COL11A1</i> , <i>SPOCK1</i> , <i>THBS2</i> ,	286
	<i>EMILIN1</i> , and <i>TPM2</i> ), response to growth factors ( <i>INHBA</i> , <i>FGFR1</i> ,	287
	<i>HSPB1</i> ), and mesenchymal cell proliferation ( <i>LMNA</i> , <i>UACA</i> ) were	288
	the most differentially upregulated pathways in the stroma of	289
	patients with poor outcome (compared with patients with favorable	290
	outcome; Fig. 1C; Supplementary Table S4). The humoral immune	291
	response (involving genes such as <i>LCN2</i> , <i>PGC</i> , <i>REG1A</i> , <i>ITLN1</i> ,	292
	<i>BPIFB1</i> , and <i>BIRC3</i> ), digestive tract development ( <i>GATA6</i> , <i>ITGA6</i> ,	293
	<i>CLDN18</i> ), and tissue homeostasis ( <i>LYZ</i> , <i>MUC6</i> ) were most signifi-	294
	cantly downregulated in these patients' stroma, compared with	295
	patients with favorable outcome (Fig. 1C; Supplementary Table S4).	296
	Analysis of cancer samples from the same patients highlighted only 13	297
	DEGs, and no significant differentially regulated pathways (Supple-	298
	mentary Table S3; Supplementary Fig. S1H).	299
	The observed changes in stromal gene expression could be driven by	300
	differences in stromal abundance between the patient groups. To test	301
	this, we performed image analysis to quantify stroma, cancer, and	302
	immune regions in hematoxylin & eosin (H&E) stained FFPE sections	303
	from the patients. We found no significant difference in the percentage	304
	of stroma, cancer, and immune cells between the favorable and poor	305
	outcome patients, suggesting that it is not the abundance, but the	306
	transcriptional program that is different between the two groups	307
	(Supplementary Figs. S1I–S1L). These findings suggest that as tumors	308
	progress, stromal pathways involved in maintaining normal stomach	309
	functions are replaced by pathways resulting from tumor–stroma	310
	interactions that support tumor growth.	311
	We next set out to test the correlation between our stromal signature	312
	and clinical characteristics in independent datasets. Because no pure	313
	gastric CAF datasets with reported disease outcome are available, to the	314
	best of our knowledge, we turned to published datasets from bulk	315
		316
		317

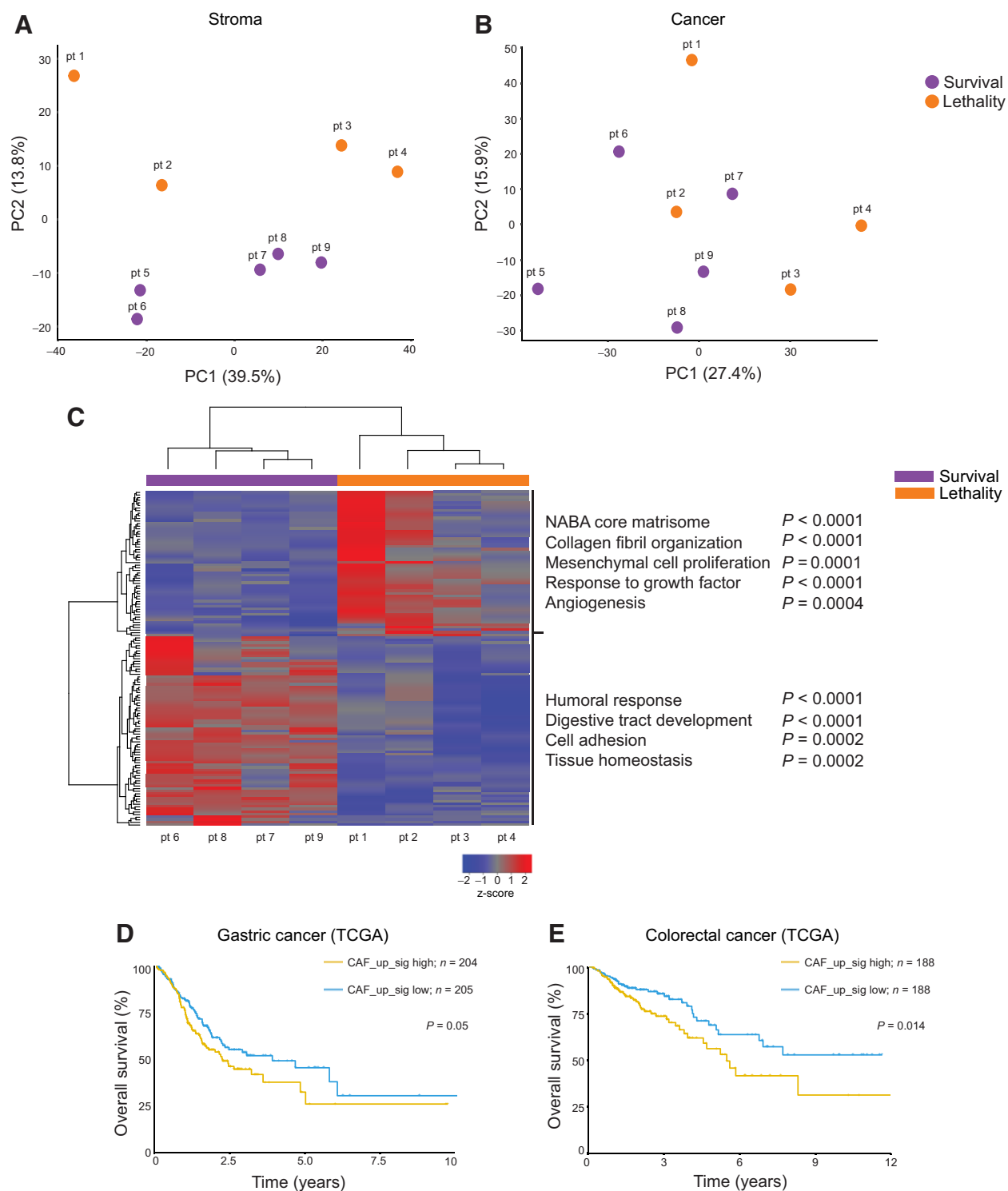


**Figure 1.**

The transcriptional landscape of gastric cancer stroma changes with disease aggressiveness. CAF-rich or cancer-rich regions of tumor sections from 9 patients with gastric cancer were laser-capture microdissected and analyzed by RNA-seq. PCA was performed for (A) CAFs and (B) cancer cells. Purple/orange dots—survival/lethality, as indicated. C, Heatmap showing hierarchical clustering of 129 genes differentially expressed in CAF-rich samples with favorable versus poor outcome. Pathway analysis was performed using Metascape. Selected significant pathways ( $P < 0.05$ , FDR  $< 0.5$ ) are shown (see Supplementary Table S4). Purple/orange bars—survival/lethality, as indicated. D and E, Kaplan-Meier (KM) analysis showing overall survival of patients with (D) gastric or (E) colorectal cancer from the TCGA stratified on the basis of median expression of the stromal gene signature (CAF\_up\_sig).

Q5

tumors and asked whether a stromal signature comprised of genes upregulated in poor outcome patients in our dataset (CAF\_up\_sig) could be detected in bulk tumors (including both stroma and cancer cells). First, we analyzed The Cancer Genome Atlas (TCGA) datasets for gastrointestinal (GI) tract cancers (gastric, colorectal, pancreatic, hepatocellular, esophageal; Fig. 1D–E; Supplementary Table S5), and found that the CAF\_up\_sig is significantly associated with poor outcome in gastric cancer and in colorectal cancer (Fig. 1D and E). Genes downregulated in the stroma (CAF\_down\_sig) did not show any significant association with survival (Supplementary Figs. S1M and S1N).

We then analyzed datasets from three other large patient cohorts: The Singapore cohort, the KUGH\_KUCM cohort, and the ACRG cohort (Supplementary Table S6). CAF\_up\_sig expression significantly associated with poor overall survival in the Singapore cohort and in the KUGH\_KUCM cohort, and a similar trend was found with the ACRG cohort (Fig. 2A–C). Our CAF\_down\_sig showed an opposite trend – high expression of CAF\_down\_sig significantly correlated with favorable outcome in the Singapore and KUGH\_KUCM cohorts, and a similar mild trend was observed with the ACRG cohort (Fig. 2D–F). Univariate analysis showed that CAF\_up\_sig expression, cancer stage, and presence of metastasis were associated with poor overall survival in the Singapore and the KUGH\_KUCM cohorts and the ACRG cohort showed a similar trend (Supplementary Table S6).

We next looked for potential associations between expression of our CAF signature and gastric cancer subtypes. In all 3 patient datasets, CAF\_up\_sig expression, but not CAF\_down\_sig expression, was significantly enriched in the diffuse gastric cancer subtype, which typically has a worse prognosis compared with the intestinal subtype (Fig. 2G–I; Supplementary Figs. S2A–S2C). In addition to the histologic classification of gastric cancer to diffuse and intestinal subtypes, two independent molecular classification methods were described recently (4, 5): A mesenchymal phenotype (MP) characterized by high genomic integrity and associated with poor survival, and an epithelial phenotype (EP) characterized by low genomic integrity and associated with favorable survival, were identified in the KUGH\_KUCM cohort (5); and four molecular subtypes (MSS TP53<sup>-</sup>, MSS TP53<sup>+</sup>, MSI, EMT) were characterized in the ACRG cohort, of which the EMT subtype was associated with the worst outcome (4). Analyzing the KUGH\_KUCM cohort, we found that the CAF\_up\_sig was significantly enriched in the MP class, and the CAF\_down\_sig was significantly enriched in the EP class (Fig. 2J). In the ACRG cohort, the CAF\_up\_sig was significantly enriched in the EMT subtype while the CAF\_down\_sig was significantly enriched in MSS TP53<sup>+/-</sup> subtypes, associated with more favorable outcomes (Fig. 2K).

Supporting this classification, gene set enrichment analysis (GSEA) using MSigDB (Hallmark gene sets, see Supplementary Materials and Methods) on the full stromal RNA-seq dataset highlighted EMT as the most significantly enriched pathway in patients with poor outcome compared with patients with favorable outcome (Supplementary Figs. S2D; Supplementary Table S7). These analyses collectively indicate that the stromal signature correlates with diffuse, mesenchymal, and aggressive gastric cancer subtypes, further reinforcing the clinical relevance of our stromal classification and pointing to specific genes for dissection and targeting.

**A transcriptional signature derived from mouse PDPN<sup>+</sup> gastric CAFs is associated with aggressive gastric cancer phenotypes and poor disease outcome in patients**

To further dissect the contribution of CAFs to gastric cancer, we induced gastric cancer in mice using a triple-transgenic gastric cancer

mouse model- Lgr5-EGFP-IRES-CreERT2; R26-LSL-rtTA-IRES-EGFP; tetO-GLI2A mice, (iLgr5;GLI2A mice; ref. 21). This model is based on deregulated activation of the Hedgehog pathway by expression of GLI2A, an activated form of GLI2, in Lgr5 expressing stem cells in the stomach (21). We isolated CAFs and normal fibroblasts from the stomachs of gastric cancer-induced and naïve iLgr5;GLI2A mice, and performed RNA-seq to obtain a pure mouse CAF transcriptional signature (Supplementary Table S8). To that end tumors were excised 3 weeks after GLI2A induction, and CAFs were isolated by fluorescence activated cell sorting (FACS) based on negative selection for CD45 (immune), EpCAM (epithelial), and CD31 (endothelial cells), and positive selection for PDPN (fibroblasts; Supplementary Fig. S3A; Supplementary Table S9; refs. 16, 28, 29). A total of 154 genes were differentially upregulated and 207 were differentially downregulated in CAFs compared with normal gastric fibroblasts (Supplementary Table S8). Pathway analysis highlighted similar pathways to those discovered in the stromal dissection of the human patient samples: ECM organization (*Adam12, Acan, Lox*), activation of matrix metalloproteinases (*Mmp3, Mmp9, Mmp10, Mmp13*), response to growth factors (*Inhba, Grem1, Runx3*), and regulation of hormone levels (*Inhba, Cnr1, Cpe*) were among the most differentially upregulated pathways in mouse CAFs, whereas digestion (*Apoa1, Tff1, Pgc*) and tissue homeostasis (*Atp4a, Car2, Cldn18*) were the most differentially downregulated pathways compared with normal gastric fibroblasts (Supplementary Table S10). We then checked whether a signature comprised of genes upregulated in mouse CAFs (mCAF\_up\_sig) or genes downregulated in mouse CAFs (mCAF\_down\_sig) would be associated with clinical characteristics in the Singapore, KUGH\_KUCM, and ACRG cohorts (Supplementary Table S11). Similar to the CAF\_up\_sig from patient samples, high expression of the mCAF\_up\_sig significantly associated with poor overall survival in the Singapore cohort and in the KUGH\_KUCM cohort, and the ACRG cohort showed a similar trend that was not statistically significant (Fig. 3A; Supplementary Figs. S3B and S3C). The mCAF\_down\_sig showed an opposite trend—it was significantly associated with favorable outcome in the Singapore cohort and a similar trend was seen in the KUGH\_KUCM cohort (Fig. 3A; Supplementary Fig. S3D). The ACRG cohort showed no particular trend for this analysis (Supplementary Fig. S3E). The mCAF\_up\_sig also correlated with the more aggressive MP and EMT molecular subtypes similar to the CAF\_up signature from patient samples (Fig. 3B; Supplementary Fig. S3F), whereas the mCAF\_down\_sig correlated with the less aggressive EP and MSS TP53<sup>+/-</sup> subtypes (Fig. 3B; Supplementary Fig. S3G). Collectively, the findings obtained from pure mouse CAFs support our findings from patient samples, indicate that CAFs support gastric cancer and provide potential targets and experimental systems for further characterization in mouse and human.

**INHBA and THBS1/2 are upregulated in gastric cancer stroma**

To characterize stromal pathways highlighted by our transcriptional profiling, we queried our patient gene list for potential interactions of translated proteins using STRING (Fig. 3C). On the basis of this analysis we chose to focus on two targets upregulated in poor outcome patients: inhibin Subunit Beta A (INHBA) and thrombospondin 2 (THBS2), suggested to be part of a common signaling network (30). Both targets were recently found by us to be highly expressed in a subset of wound-healing CAFs in breast cancer (16). Moreover, they were both part of the EMT gene set highlighted by the GSEA analysis as enriched in patients with poor outcome (Supplementary Fig. S2D; Supplementary Table S7). We added to this analysis thrombospondin 1 (THBS1), a close homologue of THBS2 that showed a similar trend of

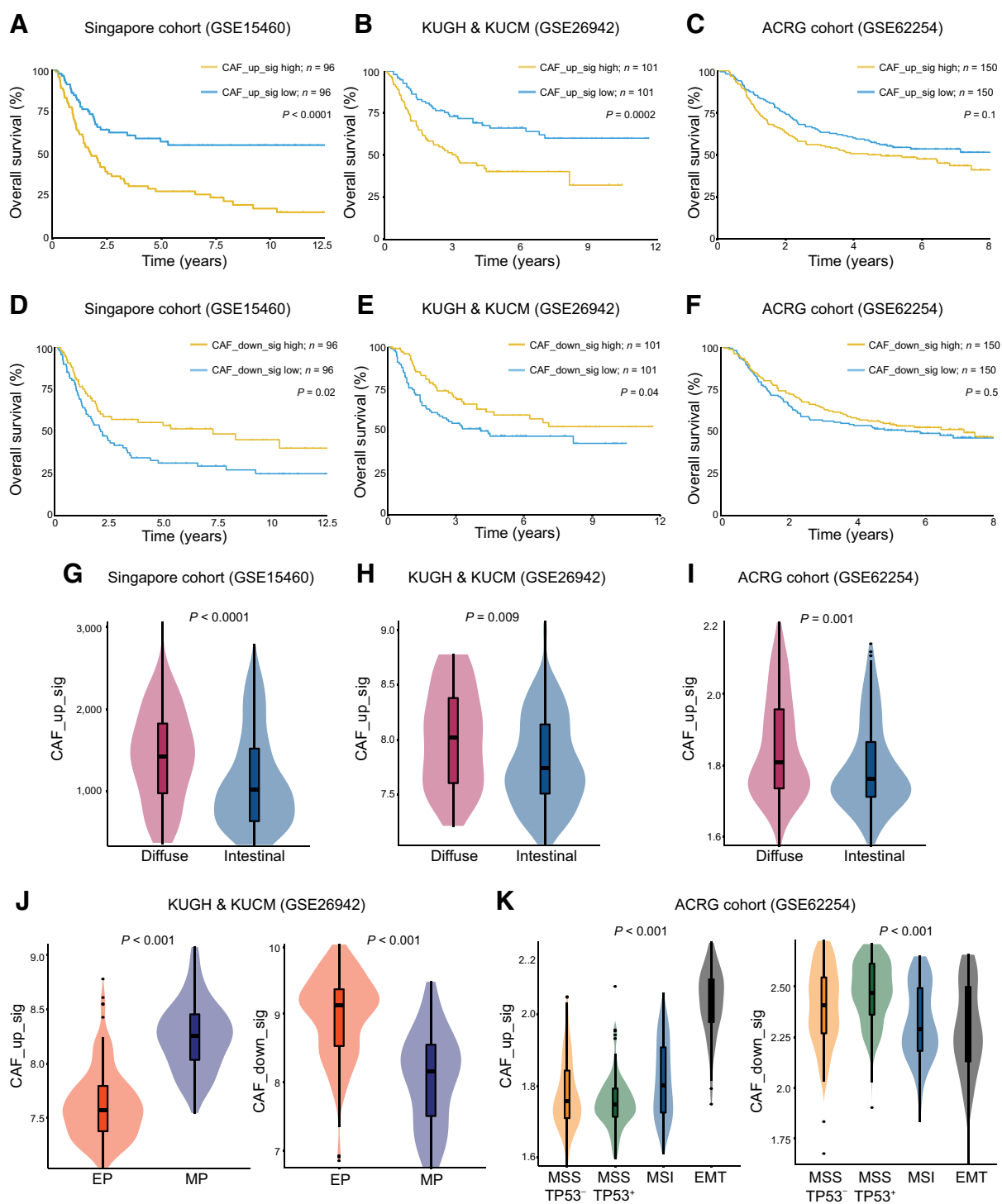
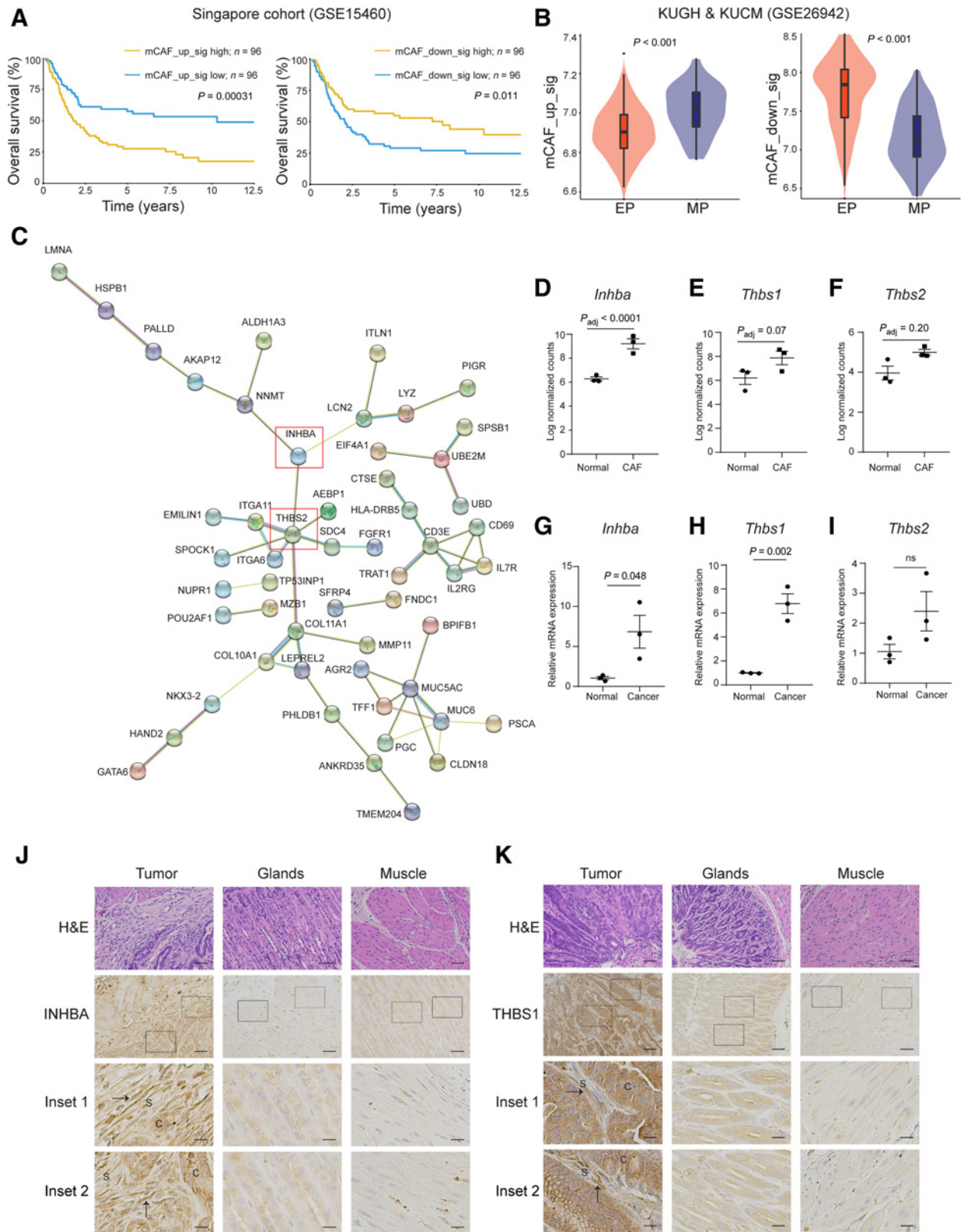


**Figure 2.**

High expression of the CAF signature is associated with aggressive disease and poor disease outcome in patients with gastric cancer. **A–C**, KM analysis showing overall survival of patients from **(A)** the Singapore cohort; **(B)** the KUGH & KUCM cohort; and **(C)** the ACRG cohort stratified on the basis of expression of the upregulated (CAF\_up\_sig) stromal gene signature. **D–F**, KM analysis showing overall survival of patients from the **(D)** Singapore cohort, **(E)** KUGH & KUCM cohort, and **(F)** ACRG cohort stratified on the basis of expression of the downregulated (CAF\_down\_sig) stromal gene signature. **G–I**, Enrichment of the CAF\_up\_sig (mean of normalized counts) in patients with diffuse versus intestinal gastric cancer in the **(G)** Singapore cohort; **(H)** KUGH & KUCM cohort; and **(I)** ACRG cohort. **J**, Enrichment of the CAF\_up\_sig and CAF\_down\_sig (mean of the normalized counts) in patients with MP and EP subtypes in the KUGH & KUCM cohort (5). **K**, Enrichment of the CAF\_up\_sig and CAF\_down\_sig (mean of normalized counts) in patients with molecular subtypes previously identified in the ACRG cohort (4). One-way ANOVA was used in **G–K**.







443 expression (Supplementary Table S3) and was also included in the  
 444 enriched EMT gene set (Supplementary Table S7). *Inhba* was differ-  
 445 entially upregulated also in mouse CAFs from *iLgr5;GLI2A* tumors,  
 446 and *Thbs1/2* showed a similar trend (Fig. 3D–F). *INHBA* is a subunit  
 447 of Activin and Inhibin, dimeric proteins belonging to the TGFβ  
 448 superfamily (31, 32). Activin A is a homodimer of two *INHBA*  
 449 subunits, whereas Inhibin A and Activin AB are heterodimers of  
 450 *INHBA* with *INHBA* and *INHBB*, respectively (32). *INHBA* is known to  
 451 play a role in inflammation, tissue repair, and activation of myofi-  
 452 broblasts, and increased levels of *INHBA* are associated with lymph  
 453 node (LN) metastasis, gastric cancer cell proliferation and chemore-  
 454 sistance (33). *THBS1/2* are adhesive glycoproteins involved in cell–cell  
 455 and cell–matrix interactions. Increased levels of *THBS2* are associated  
 456 with LN metastasis and increased invasion in gastric cancer (34). The  
 457 role of *THBS1* is less clear since it was implicated both in pro- and  
 458 antitumorogenic activities in gastric cancer (35–37). Both *INHBA* and  
 459 *THBS1/2* are known to play an important role in gastric cancer,  
 460 however their role in the TME is not well studied (30). To validate  
 461 our RNA-seq results, we extracted total RNA from *iLgr5;GLI2A*  
 462 tumors and examined the levels of *Inhba*, *Thbs1*, and *Thbs2* by qPCR.  
 463 *Inhba* and *Thbs1* levels were significantly upregulated in gastric tumors  
 464 compared with normal gastric tissue and *Thbs2* showed a similar trend  
 465 (Fig. 3G–I). To define the tissue localization of *INHBA* and *THBS1/2*,  
 466 and confirm their expression at the protein level, we performed IHC  
 467 staining of sections from *iLgr5;GLI2A* tumors and from normal  
 468 stomach controls using antibodies against *INHBA* and *THBS1*.  
 469 *INHBA* and *THBS1* were expressed at very low levels in normal  
 470 gastric glands and muscle (Fig. 3J and K). Gastric tumors, however,  
 471 exhibited high levels of *INHBA* and *THBS1* both in stroma and in  
 472 cancer cells (Fig. 3J and K). Together, these findings support our  
 473 patient RNA-seq results and suggest that *INHBA* and *THBS1/2* are  
 474 upregulated in gastric cancer stroma.

475 Given their connectivity to other genes in the stromal network  
 476 revealed by the STRING analysis (Fig. 3C), and the potential simplicity  
 477 of a 3-gene signature (compared with a signature comprised of dozens  
 478 of genes), we tested whether a minimal gene signature comprised of  
 479 only *INHBA* and *THBS1/2* would correlate with disease outcome in  
 480 our patient datasets. We found that the 3-gene signature (*INHBA*/  
 481 *THBS1/THBS2*) correlated with poor disease outcome in the TCGA  
 482 gastric cancer and colorectal cancer datasets, the Singapore cohort,  
 483 and the KUGH\_KUCM cohort (Supplementary Figs. S4A–S4D; Supple-  
 484 mentary Table S6). As with the other stromal signatures that we  
 485 analyzed, the ACRG cohort showed a similar trend of disease outcome  
 486 that was not statistically significant (Supplementary Fig. S4E), possibly  
 487 due to differences in patient follow up time or cohort characteristics  
 488 (Supplementary Table S6). These results imply that stromal *INHBA*  
 489 and *THBS1/2* are associated with aggressive disease phenotypes in  
 490 gastric cancer, and serve as attractive targets for characterization.

### HSF1 activation in gastric CAFs is associated with poor disease outcome

492 In search for potential transcriptional regulators of the stromal  
 493 signature in general, and *INHBA* and *THBS1/2* in particular, we  
 494 examined heat-shock factor 1 (HSF1). Previously, we and others have  
 495 shown that HSF1, the master transcriptional regulator of the heat  
 496 shock response, plays an important role in the conversion of fibroblasts  
 497 into CAFs in the TME (20, 38). Moreover, *INHBA* and *THBS1* were  
 498 shown to be transcriptional targets of HSF1 (39, 40). In gastric cancer,  
 499 activation of HSF1 in cancer cells was shown to correlate with poor  
 500 disease outcome (41), yet the contribution of stromal HSF1 to disease  
 501 outcome has not been assessed. HSF1 translocates from the cytoplasm  
 502 to the nucleus and binds to heat shock elements in the DNA upon  
 503 activation (39). Therefore, its nuclear localization is commonly used as  
 504 a proxy for HSF1 activation (39). Indeed, IHC staining of FFPE  
 505 sections from patients with gastric cancer revealed nuclear HSF1  
 506 staining both in cancer cells and in CAFs, whereas normal stomach  
 507 glands and muscle exhibited low or no HSF1 staining (Fig. 4A).  
 508

509 To systematically test whether stromal activation of HSF1 is asso-  
 510 ciated with disease outcome in gastric cancer, we performed IHC  
 511 staining for HSF1 and scored its nuclear localization in cancer cells and  
 512 CAFs, in sections from 64 patients with gastric cancer (including the  
 513 subcohort of LCM-RNA-seq patients) with documented clinical  
 514 characteristics and patient outcome data (Supplementary Table S1).  
 515 High HSF1 activation in cancer cells correlated with shorter overall  
 516 survival time and stromal HSF1 showed a similar trend (Fig. 4B and C;  
 517 Supplementary Table S12). In the cohort of patients analyzed by LCM  
 518 and RNA-seq, all patients with poor outcomes also exhibited inter-  
 519 mediate or high HSF1 activation (i.e., nuclear localization) in cancer  
 520 and stromal cells, whereas patients with favorable outcomes differed in  
 521 their HSF1 activation status (Supplementary Table S1). Interestingly,  
 522 stromal HSF1 activation also significantly correlated with HER2 status  
 523 —HER2<sup>−</sup> patients exhibited high HSF1 levels whereas HER2<sup>+</sup> patients  
 524 had low stromal HSF1 activation levels (Supplementary Table S1).  
 525 These results imply that in addition to its previously described roles  
 526 in gastric cancer cells, HSF1 activates complementary pathways in  
 527 gastric stroma that promote aggressive disease phenotypes. This  
 528 conclusion was further supported by a multivariate Cox proportional  
 529 hazards regression analysis (Supplementary Table S12). In an additive  
 530 multivariate model considering tumor stage and HSF1 score, stromal  
 531 HSF1 score and tumor stage were significantly associated with overall  
 532 survival ( $P = 0.006$ ), and this association was more significant than  
 533 that of cancer HSF1 and tumor stage with survival ( $P = 0.016$ ).  
 534

### Stromal *INHBA* and *THBS1/2* are targets of HSF1, *in vitro*

535 Multiplexed immunofluorescent staining (MxIF) of patient with  
 536 gastric cancer samples showed that HSF1 is co-expressed with *INHBA*  
 537 and *THBS1*, in cancer cells and in CAFs, whereas normal stomach  
 538

**Figure 3.**

*INHBA* and *THBS1/2* are upregulated in gastric cancer. **A** and **B**, Gastric cancer was induced in *iLgr5;GLI2A* mice, PDPN<sup>+</sup> fibroblasts were isolated from the resulting tumors and RNA-seq was performed using fibroblasts isolated from stomachs of naïve mice as control. Signatures comprised of genes upregulated (mCAF\_up\_sig;) or downregulated (mCAF\_down\_sig) in PDPN<sup>+</sup> CAFs vs. PDPN<sup>+</sup> normal fibroblasts were derived. **A**, KM analysis of overall survival in patients from the Singapore cohort stratified on the basis of expression of the mCAF\_up\_sig (left) or mCAF\_down\_sig (right). **B**, Enrichment of the mCAF\_up\_sig and mCAF\_down\_sig (mean of normalized counts) in patients with the MP and EP subtypes in the KUGH & KUCM cohort. One-way ANOVA was used for statistical analysis. **C**, STRING analysis of potential interactions between protein products of genes differentially expressed in patients with gastric cancer with favorable versus poor outcome. Proteins with no connections were omitted from the image. *THBS2* and *INHBA* are highlighted in red. **D–F**, Log-normalized counts and  $P$ -adjusted values of the indicated genes taken from DESeq analysis of the *iLgr5;GLI2A* PDPN<sup>+</sup> CAF RNA-seq data (Supplementary Table S8). **G–I**, Total RNA levels of the indicated genes normalized to HPRT in normal stomachs and tumors (cancer) from *iLgr5;GLI2A* mice.  $N = 3$  mice per group, means  $\pm$  SEM are presented. Two-tailed Student  $t$  test was used for statistical analysis. **J–K**, Representative images showing H&E and immunohistochemical staining of the indicated proteins in gastric tumors and control stomachs (naïve) from *iLgr5;GLI2A* mice.  $N = 5$  mice for cancer and  $N = 3$  mice for normal control. C, cancer; S, stroma. Scale bar = 100  $\mu$ m. Arrows indicate *INHBA* and *THBS1* positive CAFs.

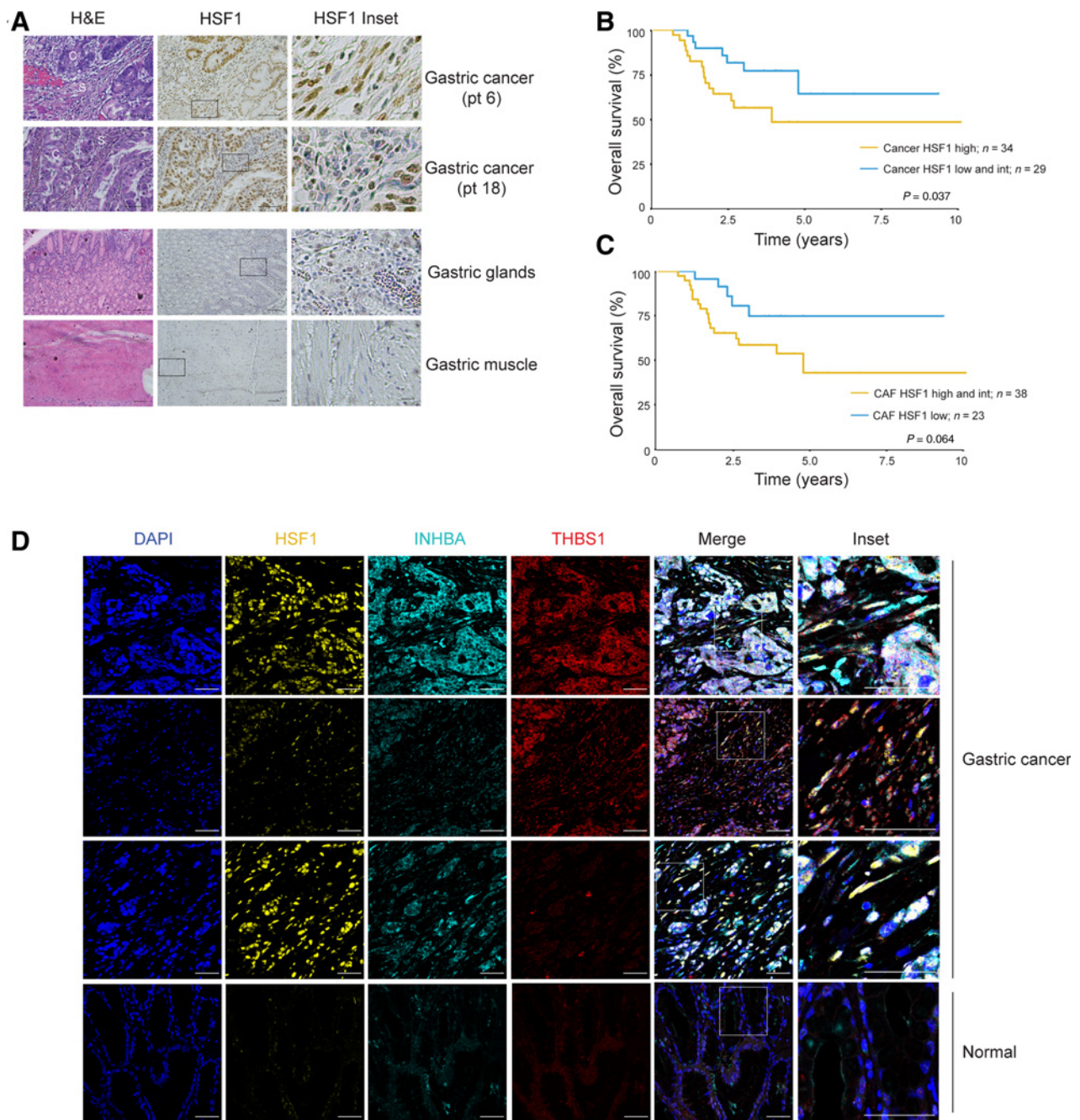


**Figure 4.**

HSF1 is co-expressed with INHBA and THBS1 in human gastric CAFs. **A**, FFPE sections from 64 patients with gastric cancer and four normal controls were stained by H&E and IHC staining for HSF1. (Top) Images representing high (pt 6) versus low (pt 18) nuclear HSF1 staining in CAFs. (Bottom) Representative images of normal gastric glands and muscle. C, cancer; S, stroma. Scale bar = 100  $\mu\text{m}$ . **B** and **C**, 64 gastric cancer samples stained as described above were scored for high/intermediate (int)/low nuclear HSF1 staining in cancer cells/CAFs, and KM analysis of overall survival in these patients was performed. **B**, Patients were stratified by high versus int/low HSF1 scores in cancer cells. **C**, Patients were stratified by high/int versus low HSF1 scores in CAFs (see Supplementary Table S1). **D**, FFPE sections from 4 patients with gastric cancer and 2 normal stomach controls were stained by multiplexed immunofluorescence for HSF1, INHBA, THBS1, and DAPI (nuclear marker). Representative images from 3 different patients and one control are shown. Scale bar = 50  $\mu\text{m}$ .

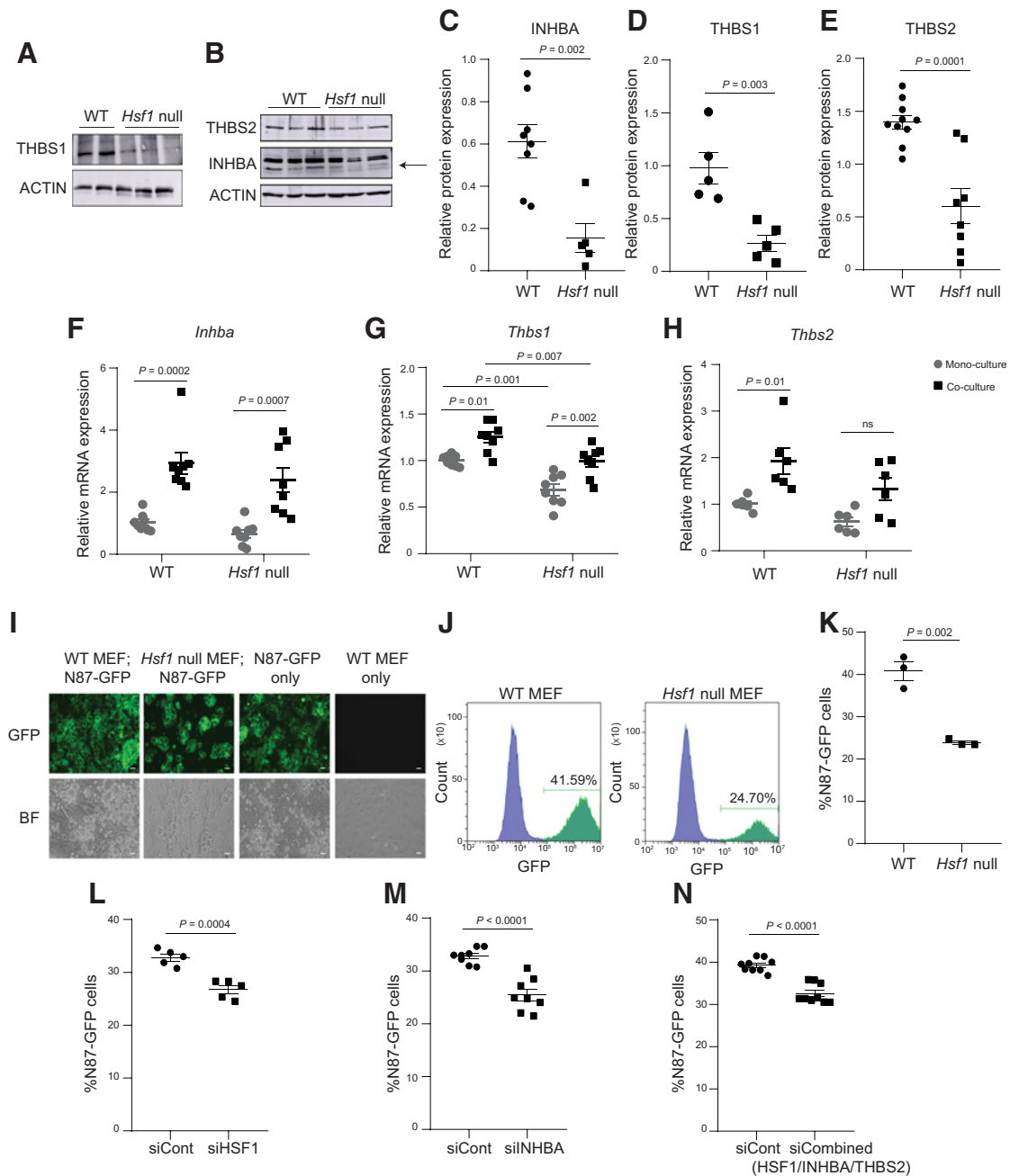


**Figure 5.**

Stromal INHBA and THBS1/2 expression is HSF1-dependent. **A–E**, INHBA, THBS1, and THBS2 protein expression levels in WT and *Hsf1* null primary MEFs were analyzed by Western blot analysis. Representative blots are shown in **A** and **B**. An arrow indicates the expected size of INHBA bands. **C**, INHBA Western blot analysis results of 5 to 10 biological replicates (across two experiments) were quantified, normalized to actin, and are presented as mean  $\pm$  SEM. **D** and **E**, THBS1 Western blot analysis results of five biological replicates (across two experiments) and THBS2 Western blot analysis results of 5 to 10 biological replicates (across three experiments) were quantified, normalized to actin, and are presented as mean  $\pm$  SEM. Two-tailed Student *t* test was used for statistical analysis in **C–E**. **F–K**, WT and *Hsf1* null MEFs were co-cultured with N87-GFP cells for 72 hours, and each cell type was grown in mono-culture as control. Co-cultures were sorted by flow cytometry using GFP. **F–H**, The levels of the indicated genes in (GFP-negative) MEFs were determined by qPCR. Average expression in six to eight biological replicates (across three experiments for *INHBA* and *THBS1* and two experiments for *THBS2*), normalized to *HPRT*,  $\pm$  SEM are presented. Two-way ANOVA was used for statistical analysis. **I**, Representative GFP (top), and brightfield (bottom) images of mono- and co-cultures are shown.  $N = 3$  biological replicates. Scale bar = 50  $\mu$ m. **J**, Representative FACS plots showing the percentage of N87-GFP cells co-cultured with WT (left) and *Hsf1* null MEFs (right).  $N = 3$  biological replicates. **K**, The average percentage ( $\pm$ SEM) of N87-GFP cells co-cultured with WT and *Hsf1* null MEFs in three biological replicates is shown. Two-tailed Student *t* test was used for statistical analysis. **L–N**, HFF cells treated with siHSF1, siINHBA, siHSF1-INHBA-THBS2 (siCombined), or siControl as indicated were co-cultured with N87-GFP cells for 72 hours. The percentage of N87-GFP in the co-cultures averaged across five to nine biological replicates ( $\pm$ SEM; across three experiments for siINHBA and siHSF1-INHBA-THBS2 and two experiments for siHSF1) is shown. Two-tailed Student *t* test was used for statistical analysis.



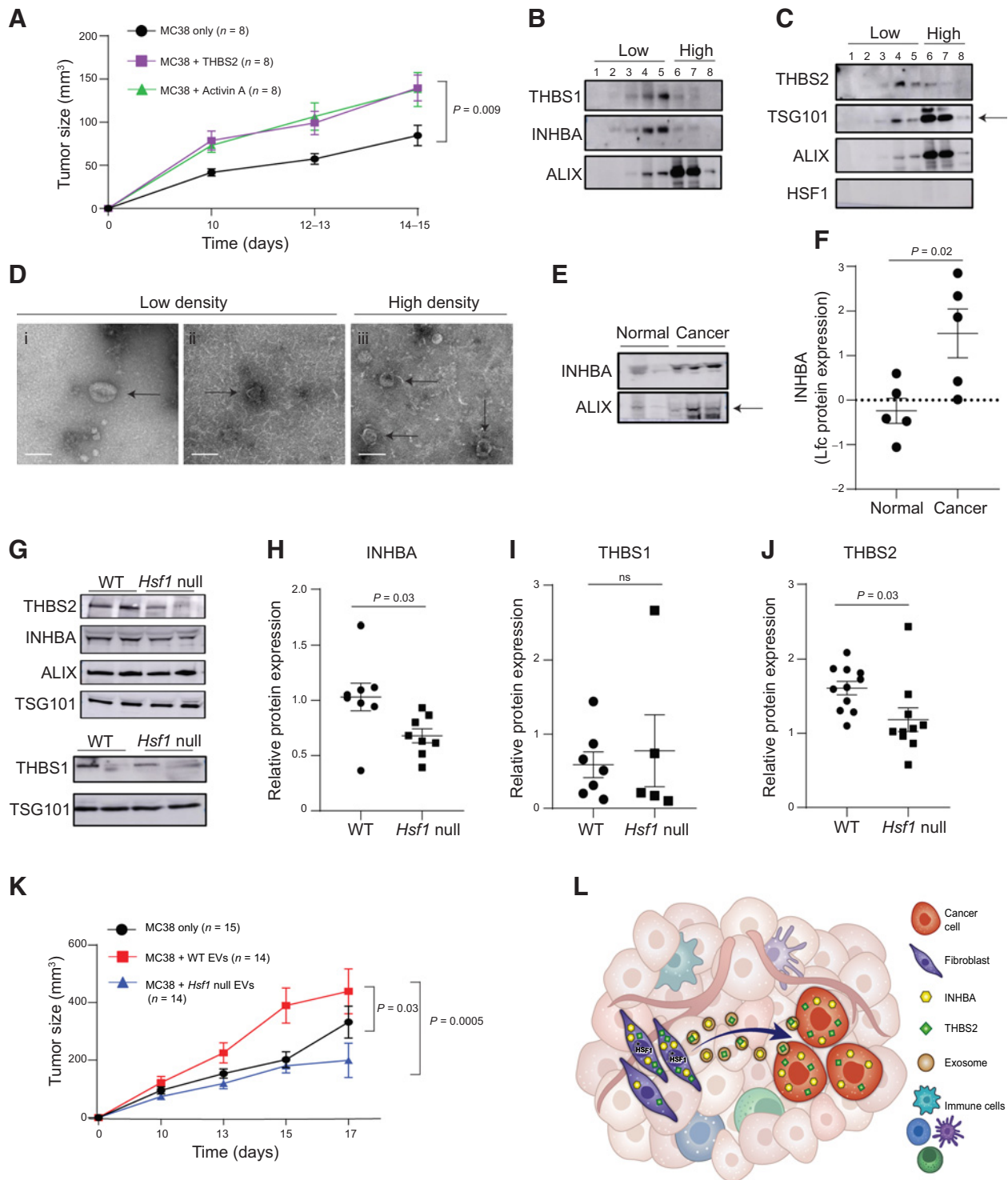


**Figure 6.**

Fibroblast-derived EVs promote tumor growth in an HSF1-dependent manner. **A**, Nude mice were injected subcutaneously with MC38 cancer cells alone, or co-injected with either recombinant THBS2 or Activin A followed by another injection of recombinant protein 2 days later. Tumor size measured by caliper is presented as mean  $\pm$  SEM for  $N = 8$  mice per group (across two experiments). Repeated measures two-way ANOVA using least-squares means to adjust for group pairwise comparisons was used for statistical analysis. **B** and **C**, Western blot analysis of fractions obtained from Optiprep density gradient isolation of EVs secreted by WT MEFs blotted against exosomal markers ALIX and TSG101, as well as THBS1/2, INHBA, and HSF1. EVs from three WT MEFs were pooled together for the isolation. The experiment was repeated twice (with different biological replicates), representative results are shown. **D**, Representative TEM images of low (i-ii) and high (iii) density EV fractions (repeated two times, from two biological replicates). (Continued on the following page.)

541 tissue exhibited low INHBA, THBS1, and HSF1 staining (Fig. 4D). To  
 542 test whether HSF1 regulates INHBA and THBS1/2 stromal expression,  
 543 and whether this regulation affects cancer cells, we measured the  
 544 expression of INHBA and THBS1/2 in WT versus *Hsf1* null mouse  
 545 embryonic fibroblasts (MEF). THBS1/2 and INHBA protein levels  
 546 were significantly higher in WT MEFs compared with *Hsf1* null MEFs  
 547 (Fig. 5A–E). Next, we asked if INHBA and THBS1/2 expression in  
 548 fibroblasts is affected by co-culture with cancer cells. Seventy-two  
 549 hours of co-culture with N87 human gastric cancer cells led to a  
 550 significant increase in *Inhba*, *Thbs1*, and *Thbs2* mRNA levels com-  
 551 pared with cells grown in mono-culture (Fig. 5F–H). Some induction  
 552 was also observed in *Hsf1* null MEFs upon co-culture, however the  
 553 total levels were lower in *Hsf1* null MEFs compared with WT MEFs  
 554 (Fig. 5F–H).

555 To determine how this stromal network affects cancer cells, we  
 556 monitored cancer cell growth in co-culture. N87 cells showed a  
 557 significant growth reduction when co-cultured with *Hsf1* null MEFs  
 558 compared with WT MEFs (Fig. 5I–K), and similar results were  
 559 observed upon co-culture of N87 cells with human foreskin fibroblasts  
 560 (HFF) in which HSF1 was knocked down by siRNA (Fig. 5L; Sup-  
 561 plementary Figs. S5A–S5C).

562 Next, we knocked down *INHBA*, *THBS1*, and *THBS2* in fibroblasts  
 563 and monitored gastric cancer cell growth in co-culture. Knockdown of  
 564 *THBS2* in HFFs led to a minor decrease in N87 cell proliferation, and  
 565 knockdown of *THBS1* led to a minor increase in N87 proliferation  
 566 (Supplementary Figs. S5D–S5F). Knockdown of *INHBA* however led  
 567 to a substantial and significant decrease in the growth of co-cultured  
 568 N87 cells (Fig. 5M; Supplementary Fig. S5G). A combined knockdown  
 569 of *HSF1*–*INHBA*–*THBS2* had a similar effect on N87 growth (Fig. 5N),  
 570 whereas the combination of *HSF1* and *INHBA* with *THBS1* had a  
 571 milder effect (Supplementary Fig. S5H). Collectively, these results  
 572 support the hypothesis that HSF1, INHBA, and THBS1/2 are part of  
 573 a common stromal protumorigenic signaling network, in which HSF1  
 574 regulates the expression of *THBS1/2* and *INHBA*. Although INHBA  
 575 and THBS2 seem to play a protumorigenic role in fibroblasts, THBS1  
 576 may be antitumorigenic.

577 **THBS2 and INHBA are secreted from fibroblasts via EVs, in an**  
 578 **HSF1-dependent manner**

579 INHBA and THBS1/2 are secreted proteins (42). We therefore  
 580 hypothesized that INHBA and THBS2 are secreted from CAFs to the  
 581 TME where they act on cancer cells, and that this process could be  
 582 mimicked by exogenous treatment with recombinant proteins. To test  
 583 this, we co-injected MC38 colon cancer cells with recombinant  
 584 proteins into mice, subcutaneously, followed by another injection of  
 585 recombinant protein 2 days later, and monitored tumor growth. Co-  
 586 injection of either THBS2 or Activin A (a homodimer of two INHBA  
 587 subunits; ref. 31) with MC38 cancer cells significantly increased the  
 588 tumorigenicity of these cells—larger and faster growing tumors  
 589 formed in the presence of THBS2 or Activin A (Fig. 6A).

590 INHBA and THBS1/2 have been proposed to shuttle through  
 591 EVs (43–49). Recently, THBS2 was shown to be a marker for exosomes  
 592 secreted by tumors (50). We therefore hypothesized that the protu-  
 593 morigenic effects of stromal HSF1 may be mediated by secretion and  
 594 delivery of these proteins to the TME, possibly via EVs. Small EVs are  
 595 lipid bilayer-enclosed particles sized 30 to 150 nm, which mediate cell-  
 596 cell communication via targeting, fusion, and release of content from  
 597 one cell to another (51). Their cargo includes bioactive molecules such  
 598 as effector proteins, metabolites, large and small RNAs, and even  
 599 genomic DNA (50). Recently, EVs secreted from stromal cells were  
 600 shown to contribute to disease progression and poor disease outcome  
 601 by promoting vascularization and chemotherapy resistance (52). To  
 602 test whether INHBA and THBS1/2 are secreted via EVs in an HSF1-  
 603 dependent manner, we first confirmed the presence of INHBA and  
 604 THBS1/2 in EVs by OptiPrep density gradient isolation of EVs  
 605 secreted from WT MEFs (Fig. 6B and C; Supplementary Fig. S6A).  
 606 ALIX and TSG101, two known exosome markers, were used as positive  
 607 loading controls (53). HSF1 is not expected to be found in EVs and  
 608 therefore served as a negative control. ALIX and TSG101 were found in  
 609 fractions 3 to 8. Both proteins peaked in high density fractions (6–7),  
 610 and TSG101 had an additional peak in low density fraction 4 (Fig. 6B  
 611 and C). HSF1 was not detected in any of these fractions. INHBA and  
 612 THBS1/2, however, were detected in fractions 2 to 7, and peaked in  
 613 fractions 4 to 5 (Fig. 6B and C). To confirm that these fractions contain  
 614 EVs, we performed transmission electron microscope (TEM) analysis.  
 615 We found that EVs are indeed observed in both low- and high-density  
 616 fractions (Fig. 6D). These observations suggest that two populations of  
 617 EVs are secreted by MEFs—a low-density population, enriched in  
 618 INHBA and THBS1/2 (Supplementary Fig. S6A) and a high-density  
 619 population with lower levels of INHBA and THBS1/2. We also checked  
 620 the presence of INHBA and THBS1/2 in EVs isolated from the serum  
 621 of *iLgr5;GLI2A* mice. Although we could not detect THBS1/2 in the  
 622 serum (possibly due to low sensitivity of the assay), INHBA was  
 623 detected, and its levels were significantly higher in EVs isolated from  
 624 the serum of tumor-bearing *iLgr5;GLI2A* mice compared with EVs  
 625 isolated from the serum of naïve *iLgr5;GLI2A* mice (Fig. 6E and F).

626 We then compared the expression levels of INHBA and THBS1/2 in  
 627 EVs isolated from WT versus *Hsf1* null fibroblasts. Although THBS1  
 628 levels were similar between WT and *Hsf1* null-derived EVs, THBS2  
 629 and INHBA levels were significantly higher in EVs derived from WT  
 630 MEFs compared with EVs from *Hsf1* null MEFs (Fig. 6G–J). These  
 631 results suggest that INHBA and THBS2 expression in EVs is HSF1-  
 632 dependent.

633 To examine whether the differential expression of INHBA and  
 634 THBS2 was due to impaired EV biogenesis in *Hsf1* null MEFs, we  
 635 compared the number and size of EVs produced by each genotype  
 636

(Continued.) (i) 1.03% sucrose; (ii) 1.04% sucrose; (iii) 1.07% sucrose. Scale bars = 100 nm. **E**, Representative Western blot analysis showing INHBA levels from EVs isolated from the serum of tumor-bearing and naïve *iLgr5;GLI2A* mice. ALIX was used as loading control. Arrow indicates expected size of ALIX. **F**, INHBA levels from EVs isolated from the serum of tumor-bearing and naïve *iLgr5;GLI2A* mice were analyzed using Western blot analysis. INHBA levels were normalized to ALIX. Average expression of INHBA normalized to ALIX in five biological replicates (across two experiments) is presented as mean ± SEM. Two-tailed Student *t* test was used for statistical analysis. **G–J**, INHBA, THBS1, and THBS2 levels in EVs derived from WT and *Hsf1* null primary MEFs were analyzed using Western blot analysis. ALIX and TSG101 were used as loading controls. Representative blots are shown in **G**, **H**. Average expression of INHBA normalized to TSG101 in eight biological replicates (across three experiments for INHBA) is presented as mean ± SEM. **I**, Average expression of THBS1 normalized to TSG101 in five to seven biological replicates (across three experiments) is presented as mean ± SEM. **J**, Average expression THBS2 normalized to TSG101 in 10 to 11 biological replicates (across four experiments) is presented as mean ± SEM. Two-tailed Student *t* test was used for statistical analysis in **H** and **I**. **K**, Nude mice were injected subcutaneously with MC38 cancer cells alone, or co-injected with EVs derived from WT or *Hsf1* null MEFs. Tumor size measured by caliper is presented as mean ± SEM for *N* = 14 to 15 mice per group (across four experiments). Repeated measures two-way ANOVA using least-squares means to adjust for group pairwise comparisons was used for statistical analysis. **L**, Graphic summary of the proposed model. HSF1 in CAFs regulates expression of INHBA and THBS1/2. INHBA and THBS2 from CAFs are packaged into EVs and secreted to the TME, where they are taken up by cancer cells.

639 using nanoparticle tracking analysis (NTA). We could not detect  
 640 differences in size or in quantity between EVs secreted from WT and  
 641 *Hsf1* null fibroblasts (Supplementary Figs. S6B–S6E). We extended our  
 642 analysis to field-flow fractionation (FFF), to better separate EV popu-  
 643 lations and assess smaller EV populations shown to be biologically  
 644 active (54). Similar to our NTA analysis, FFF did not detect consistent  
 645 differences between EVs derived from *Hsf1* null MEFs compared with  
 646 WT MEFs (Supplementary Fig. S6F). We next tested whether the  
 647 differences in protein content could be due to impaired uptake of EVs  
 648 derived from *Hsf1* null compared with WT MEFs. We incubated  
 649 N87 gastric cancer cells and MC38 colon cancer cells with CFSE  
 650 stained EVs, and analyzed uptake 12 to 16 hours later by imaging the  
 651 cells in an ImageStream imaging flow cytometer. We could not detect  
 652 differences in the percentage of CFSE<sup>+</sup> N87 and MC38 cells incubated  
 653 in the presence of EVs from *Hsf1* null compared with WT MEFs  
 654 (Supplementary Figs. S6G–S6O), indicating that HSF1 does not affect  
 655 EV biogenesis or uptake, yet it plays an important role in the protein  
 656 content of EVs.

657 To assess the biological relevance of these findings we co-injected  
 658 EVs derived from WT versus *Hsf1* null MEFs together with MC38  
 659 cancer cells into nude mice, and monitored tumor growth. Co-  
 660 injection with EVs derived from WT MEFs caused a significant  
 661 increase in the growth of MC38-injected tumors (Fig. 6K). This effect  
 662 was completely abolished when EVs from *Hsf1* null MEFs were co-  
 663 injected with MC38 cells. Taken together these experiments show that  
 664 EVs derived from WT and *Hsf1* null MEFs are similar in size, quantity,  
 665 biogenesis, and uptake into cancer cells. However, there is a significant  
 666 difference in their content and, consequently, their effect on tumor  
 667 growth. These findings imply that HSF1 regulates the expression of  
 668 INHBA and THBS1/2 in stromal cells. INHBA and THBS2 are then  
 669 packaged into EVs in an HSF1-dependent manner and secreted to the  
 670 TME, where they are taken up by cancer cells and promote a more  
 671 aggressive disease phenotype (Fig. 6L).

672 **Discussion**

673 Despite recent advances in molecular subtyping, the backbone of  
 674 gastric cancer treatment remains chemotherapeutic combinations.  
 675 Molecular classifications, based largely on mutations and genomic  
 676 alterations in the cancer cells, do not translate to guide treatment  
 677 modality. Here we chose a complementary approach—searching for  
 678 transcriptional changes in the gastric TME. We defined a stromal gene  
 679 signature associated with poor disease outcome in patients, and found  
 680 a role for the stromal master transcriptional regulator HSF1 in driving  
 681 it, through exosome-mediated secretion of protumorigenic proteins  
 682 that are taken up by cancer cells to promote aggressive disease  
 683 phenotypes.

684 HSF1 was previously shown by us and others to play protumori-  
 685 genic roles in CAFs of breast, lung, and colon carcinomas (17, 20, 38).  
 686 The finding that HSF1 also acts in gastric CAFs implicates HSF1 as a  
 687 master regulator of CAF activities in carcinomas across different  
 688 tissues, and suggests that its protumorigenic effects—in gastric cancer  
 689 and other carcinomas—may be mediated via delivery of targets to the  
 690 TME in EVs.

691 INHBA and THBS1/2 are involved in tumor progression and were  
 692 shown to be co-regulated (30, 55, 56) possibly sharing common  
 693 signaling pathways. Although INHBA and THBS2 are protumori-  
 694 genic, THBS1 was proposed to exert both pro- and antitumorigenic  
 695 effects, depending on the system examined (44, 55, 57). Our findings  
 696 suggest that all three proteins are upregulated in CAFs in an HSF1-  
 697 dependent manner. Our *in vitro* experiments and mouse co-injections

with recombinant proteins show a clear protumorigenic role of Activin  
 A and THBS2, whereas the effect of stromal THBS1 on cancer cells  
 (*in vitro*) is less clear. Taken together with the finding that INHBA and  
 THBS2 are delivered into exosomes in an HSF1-dependent manner,  
 whereas THBS1 exosomal expression is not affected by HSF1 status, it  
 is possible that selective delivery of INHBA and THBS2 to exosomes  
 leads to the protumorigenic effect observed, whereas THBS1 is  
 antitumorigenic.

EV cargo includes proteins, metabolites, RNA, and genomic  
 DNA (50), which could serve as bioactive molecules in the TME. In  
 GI-tract cancers, EVs from CAFs were shown to promote cancer  
 through delivery of miRNAs to gastric cancer cells to suppress  
 ferroptosis (58), and Wnt glycoproteins to colorectal cancer cells to  
 induce cancer stemness and chemoresistance (59). In our study,  
 differential protein expression in EVs affects their activity. Although  
 biogenesis and uptake of EVs was not impaired, loss of HSF1 abolished  
 the protumorigenic effect of EVs derived from WT MEFs. Our findings  
 indicate that EV cargo is selective and the content is affected by HSF1.

Over the last years, efforts were made to identify gastric cancer  
 drivers and gene signatures that may serve as biomarkers for diagnosis  
 and treatment (3). Trastuzumab revolutionized the treatment of  
 HER2-positive gastric cancers (60), and immunotherapy has proven  
 to be an effective therapy for patients with microsatellite instability  
 (MSI; ref. 61). Other signatures, such as those associated with *Helicobacter pylori*  
 and *EBV* infections (62, 63), germline mutations of *CDH1*, mismatch repair genes  
 (64, 65), epithelial versus mesenchymal cell types (5), and MSS TP53<sup>-</sup>,  
 MSS TP53<sup>+</sup>, MSI, EMT subtypes (4) enabled associations between molecular  
 landscape and gastric cancer subtyping (3, 60). However, the TME of  
 gastric cancer in general, and the molecular composition of gastric  
 CAFs in particular, have been scarcely studied. Our profiling of CAFs  
 from patient tumors highlights stromal compositions associated with  
 the aggressive diffuse and EMT-like gastric cancer subtypes. These  
 targets should be further explored, certainly as prognostic targets and  
 hopefully as robust therapeutic targets in gastric cancer.

**Authors' Disclosures**

No disclosures were reported.

**Authors' Contributions**

**N. Grunberg:** Formal analysis, investigation, writing—original draft, writing—review and editing. **M. Pevsner-Fischer:** Formal analysis, investigation, writing—original draft, writing—review and editing. **T. Goshen-Lago:** Resources. **J. Diment:** Formal analysis, visualization. **Y. Stein:** Formal analysis, methodology. **H. Lavon:** Investigation. **S. Mayer:** Data curation, formal analysis, methodology. **O. Levi-Galibov:** Resources, formal analysis, investigation. **G. Friedman:** Resources, investigation, methodology. **Y. Ofir-Birin:** Data curation, visualization, methodology. **L. Syu:** Resources. **C. Migliore:** Resources. **E. Shimoni:** Resources, visualization, methodology. **S.M. Stemmer:** Resources, data curation, methodology, writing—review and editing. **B. Brenner:** Resources, methodology, writing—review and editing. **A.A. Dlugosz:** Resources, writing—review and editing. **D. Lyden:** Conceptualization, data curation, supervision, investigation, methodology, writing—original draft, writing—review and editing. **N. Regev-Rudzki:** Formal analysis, methodology, writing—review and editing. **I. Ben-Aharon:** Resources, formal analysis, investigation, writing—review and editing. **R. Scherz-Shouval:** Conceptualization, supervision, investigation, methodology, writing—original draft, writing—review and editing.

**Acknowledgments**

Mouse pathological evaluation was carried out by Ori Brenner (WIS). Bioinformatic analyses were assisted by Ester Feldmesser, Ron Rotkopf, and Irit Orr (WIS). We thank Raya Eilam-Altstadter for assistance with immunostaining, Andreas Moor for guidance with LCM, Rawand Hamodi for technical assistance, and members of the



761 Scherz-Shouval lab for their valuable input. R. Scherz-Shouval was supported by ISF  
 762 grants 401/17 and 1384/1, ERC grant 754320, the Israel cancer research fund, the  
 763 Abisch-Frenkel foundation, the Laura Gurwin Flug Family Fund, the Peter and  
 764 Patricia Gruber Awards, the Comisaroff Family Trust, the Estate of Annice Anze-  
 765 lewitz, and the Estate of Mordecai M. Roshwal. R. Scherz-Shouval was the incumbent  
 766 of the Ernst and Kaethe Ascher Career Development Chair in Life Sciences. A.A.  
 767 Dlugosz was supported by NIH grants R01 CA118875 and P30 CA046592.

The costs of publication of this article were defrayed in part by the payment of page  
 charges. This article must therefore be hereby marked *advertisement* in accordance  
 with 18 U.S.C. Section 1734 solely to indicate this fact.

Received August 19, 2020; revised December 22, 2020; accepted February 1, 2021;  
 published first xx xx, xxxx.

**References**

774  
 775  
 776  
 777  
 778  
 779  
 780  
 781  
 782  
 783  
 784  
 785  
 786  
 787  
 788  
 789  
 790  
 791  
 792  
 793  
 794  
 795  
 796  
 797  
 798  
 799  
 800  
 801  
 802  
 803  
 804  
 805  
 806  
 807  
 808  
 809  
 810  
 811  
 812  
 813  
 814  
 815  
 816  
 817  
 818  
 819  
 820  
 821  
 822  
 823  
 824  
 825  
 826  
 827  
 828  
 829  
 830  
 831  
 832  
 833

1. Corso S, Isella C, Bellomo SE, Apicella M, Durando S, Migliore C, et al. A comprehensive PDX gastric cancer collection captures cancer cell-intrinsic transcriptional MSI traits. *Cancer Res* 2019;79:5884–96.

2. Lordick F, Allum W, Carneiro F, Mitry E, Tabernero J, Tan P, et al. Unmet needs and challenges in gastric cancer: the way forward. *Cancer Treat Rev* 2014;40:692–700.

3. Cancer Genome Atlas Research N. Comprehensive molecular characterization of gastric adenocarcinoma. *Nature* 2014;513:202–9.

4. Cristescu R, Lee J, Nebozhyn M, Kim KM, Ting JC, Wong SS, et al. Molecular analysis of gastric cancer identifies subtypes associated with distinct clinical outcomes. *Nat Med* 2015;21:449–56.

5. Oh SC, Sohn BH, Cheong JH, Kim SB, Lee JE, Park KC, et al. Clinical and genomic landscape of gastric cancer with a mesenchymal phenotype. *Nat Commun* 2018;9:1777.

6. Tan IB, Ivanova T, Lim KH, Ong CW, Deng NT, Lee J, et al. Intrinsic subtypes of gastric cancer, based on gene expression pattern, predict survival and respond differently to chemotherapy. *Gastroenterology* 2011;141:476–U551.

7. Van Cutsem E, Sagaert X, Topal B, Haustermans K, Prenen H. Gastric cancer. *Lancet* 2016;388:2654–64.

8. Becker KF, Keller G, Hoefler H. The use of molecular biology in diagnosis and prognosis of gastric cancer. *Surg Oncol* 2000;9:5–11.

9. Tabassum DP, Polyak K. Tumorigenesis: it takes a village. *Nat Rev Cancer* 2015; 15:473–83.

10. Hanahan D, Coussens LM. Accessories to the crime: functions of cells recruited to the tumor microenvironment. *Cancer Cell* 2012;21:309–22.

11. Morihito T, Kuroda S, Kanaya N, Kakiuchi Y, Kubota T, Aoyama K, et al. PD-L1 expression combined with microsatellite instability/CD8+ tumor infiltrating lymphocytes as a useful prognostic biomarker in gastric cancer. *Sci Rep* 2019;9:4633.

12. Sahai E, Astsaturov I, Cukierman E, DeNardo DG, Egeblad M, Evans RM, et al. A framework for advancing our understanding of cancer-associated fibroblasts. *Nat Rev Cancer* 2020;20:174–86.

13. Erez N, Truitt M, Olson P, Arron ST, Hanahan D. Cancer-associated fibroblasts are activated in incipient neoplasia to orchestrate tumor-promoting inflammation in an NF-kappa B-dependent manner (vol 17, pg 135, 2010). *Cancer Cell* 2010;17:523.

14. Finak G, Bertos N, Pepin F, Sadekova S, Souleimanova M, Zhao H, et al. Stromal gene expression predicts clinical outcome in breast cancer. *Nat Med* 2008;14: 518–27.

15. Kalluri R. The biology and function of fibroblasts in cancer. *Nat Rev Cancer* 2016; 16:582–98.

16. Friedman G, Levi-Galibov O, David E, Bornstein C, Giladi A, Dadiani M, et al. Cancer-associated fibroblast compositions change with breast-cancer progression linking S100A4 and PDPN ratios with clinical outcome. *Nature Cancer* 2020.

17. Levi-Galibov O, Lavon H, Wassermann-Dozoretz R., et al. Heat Shock Factor 1-dependent extracellular matrix remodeling mediates the transition from chronic intestinal inflammation to colon cancer. *Nat Commun* 2020;11:6245.

18. Zhi KK, Shen XJ, Zhang H, Bi JW. Cancer-associated fibroblasts are positively correlated with metastatic potential of human gastric cancers. *J Exp Clin Canc Res* 2010;29:66.

19. Li BL, Jiang YM, Li GX, Fisher GA, Li RJ. Natural killer cell and stroma abundance are independently prognostic and predict gastric cancer chemotherapy benefit. *JCI Insight* 2020;5:e136570.

20. Scherz-Shouval R, Santagata S, Mendillo ML, Sholl LM, Ben-Aharon I, Beck AH, et al. The reprogramming of tumor stroma by HSF1 is a potent enabler of malignancy. *Cell* 2014;158:564–78.

21. Syu LJ, Zhao X, Zhang Y, Grachtchouk M, Demitrack E, Ermilov A, et al. Invasive mouse gastric adenocarcinomas arising from Lgr5+ stem cells are dependent on crosstalk between the Hedgehog/GLI2 and mTOR pathways. *Oncotarget* 2016;7: 10255–70.

22. McMillan DR, Xiao XZ, Shao L, Graves K, Benjamin JJ. Targeted disruption of heat shock transcription factor 1 abolishes thermotolerance and protection against heat-inducible apoptosis. *J Biol Chem* 1998;273:7523–8.

23. Yohai VJ, Zamar RH. High breakdown-point estimates of regression by means of the minimization of an efficient scale. *J Am Stat Assoc* 1988;83:406–13.

24. Maronna RA, Zamar RH. Robust estimates of location and dispersion for high-dimensional datasets. *Technometrics* 2002;44:307–17.

25. Gnanadesikan R, Kettenring JR. Robust estimates, residuals, and outlier detection with multiresponse data. *Biometrics* 1972;28:81.

26. Love MI, Huber W, Anders S. Moderated estimation of fold change and dispersion for RNA-seq data with DESeq2. *Genome Biol* 2014;15:550.

27. Jaitin DA, Kenigsberg E, Keren-Shaul H, Elefant N, Paul F, Zaretsky I, et al. Massively parallel single-cell RNA-seq for marker-free decomposition of tissues into cell types. *Science* 2014;343:776–9.

28. Maruyama S, Furuya S, Shiraishi K, Shimizu H, Akaike H, Hosomura N, et al. Podoplanin expression as a prognostic factor in gastric cancer. *Anticancer Res* 2018;38:2717–22.

29. Shindo K, Aishima S, Ohuchida K, Fujiwara K, Fujino M, Mizuuchi Y, et al. Podoplanin expression in cancer-associated fibroblasts enhances tumor progression of invasive ductal carcinoma of the pancreas. *Mol Cancer* 2013;12:168.

30. Kim H, Watkinson J, Varadan V, Anastassiou D. Multi-cancer computational analysis reveals invasion-associated variant of desmoplastic reaction involving INHBA, THBS2 and COL11A1. *BMC Med Genomics* 2010;3:51.

31. Link AS, Zheng F, Alzheimer C. Activin signaling in the pathogenesis and therapy of neuropsychiatric diseases. *Front Mol Neurosci* 2016;7.

32. Namwanje M, Brown CW. Activins and inhibins: roles in development, physiology, and disease. *Cold Spring Harb Perspect Biol* 2016;8:a021881.

33. Seeruttun SR, Cheung WY, Wang W, Fang C, Liu ZM, Li JQ, et al. Identification of molecular biomarkers for the diagnosis of gastric cancer and lymph-node metastasis. *Gastroenterol Rep (Oxf)* 2019;7:57–66.

34. Oue N, Aung PP, Mitani Y, Kuniyasu H, Nakayama H, Yasui W. Genes involved in invasion and metastasis of gastric cancer identified by array-based hybridization and serial analysis of gene expression. *Oncology* 2005;69:17–22.

35. Hong BB, Chen SQ, Qi YL, Zhu JW, Lin JY. Association of THBS1 rs1478605 T>C in 5'-untranslated regions with the development and progression of gastric cancer. *Biomed Rep* 2015;3:207–14.

36. Huang T, Wang L, Liu D, Li P, Xiong H, Zhuang L, et al. FGF7/FGFR2 signal promotes invasion and migration in human gastric cancer through upregulation of thrombospondin-1. *Int J Oncol* 2017;50:1501–12.

37. Sun C, Yuan Q, Wu D, Meng X, Wang B. Identification of core genes and outcome in gastric cancer using bioinformatics analysis. *Oncotarget* 2017;8: 70271–80.

38. Ferrari N, Ranftl R, Chicherova I, Slaven ND, Moeendarbary E, Farrugia AJ, et al. Dickkopf-3 links HSF1 and YAP/TAZ signalling to control aggressive behaviours in cancer-associated fibroblasts. *Nat Commun* 2019;10:130.

39. Mendillo ML, Santagata S, Koeva M, Bell GW, Hu R, Tamimi RM, et al. HSF1 drives a transcriptional program distinct from heat shock to support highly malignant human cancers. *Cell* 2012;150:549–62.

40. Kovacs D, Sigmond T, Hotzi B, Bohar B, Fazekas D, Deak V, et al. HSF1Base: a comprehensive database of HSF1 (heat shock factor 1) target genes. *Int J Mol Sci* 2019;20:5815.

41. Dai W, Ye J, Zhang Z, Yang L, Ren H, Wu H, et al. Increased expression of heat shock factor 1 (HSF1) is associated with poor survival in gastric cancer patients. *Diagn Pathol* 2018;13:80.

42. Uhlen M, Fagerberg L, Hallstrom BM, Lindskog C, Oksvold P, Mardinoglu A, et al. Proteomics. Tissue-based map of the human proteome. *Science* 2015;347: 1260419.

769  
 770  
 771

772  
 773

835  
 836  
 837  
 838  
 839  
 840  
 841  
 842  
 843  
 844  
 845  
 846  
 847  
 848  
 849  
 850  
 851  
 852  
 853  
 854  
 855  
 856  
 857  
 858  
 859  
 860  
 861  
 862  
 863  
 864  
 865  
 866  
 867  
 868  
 869  
 870  
 871  
 872  
 873  
 874  
 875  
 876  
 877  
 878  
 879  
 880  
 881  
 882  
 883  
 884  
 885  
 886  
 887  
 888  
 889  
 890  
 891  
 892  
 893

Q9

Q8

896	43. Becker A, Thakur BK, Weiss JM, Kim HS, Peinado H, Lyden D. Extracellular vesicles in cancer: cell-to-cell mediators of metastasis. <i>Cancer Cell</i> 2016;30:836–48.	931
897		932
898		933
899	44. Huang WT, Chong IW, Chen HL, Li CY, Hsieh CC, Kuo HF, et al. Pigment epithelium-derived factor inhibits lung cancer migration and invasion by upregulating exosomal thrombospondin 1. <i>Cancer Lett</i> 2019;442:287–98.	934
900		935
901		936
902		937
903	45. Morhayim J, van de Peppel J, Demmers JA, Kocer G, Nigg AL, van Driel M, et al. Proteomic signatures of extracellular vesicles secreted by nonmineralizing and mineralizing human osteoblasts and stimulation of tumor cell growth. <i>FASEB J</i> 2015;29:274–85.	938
904		939
905		940
906		941
907	46. Sobral LM, Bufalino A, Lopes MA, Graner E, Salo T, Coletta RD. Myofibroblasts in the stroma of oral cancer promote tumorigenesis via secretion of activin A. <i>Oral Oncol</i> 2011;47:840–6.	942
908		943
909		944
910	47. Stenina OI, Topol EJ, Plow EF. Thrombospondins, their polymorphisms, and cardiovascular disease. <i>Arterioscler Thromb Vasc Biol</i> 2007;27:1886–94.	945
911		946
912		947
913	48. Xiao M, Zhang J, Chen W, Chen W. M1-like tumor-associated macrophages activated by exosome-transferred THBS1 promote malignant migration in oral squamous cell carcinoma. <i>J Exp Clin Cancer Res</i> 2018;37:143.	948
914		949
915		950
916	49. Zhang XW, Zhou JC, Peng D, Hua F, Li K, Yu JJ, et al. Disrupting the TRIB3-SQSTM1 interaction reduces liver fibrosis by restoring autophagy and suppressing exosome-mediated HSC activation. <i>Autophagy</i> 2020;16:782–96.	951
917		952
918		953
919	50. Hoshino A, Kim HS, Bojmar L, Gyan KE, Cioffi M, Hernandez J, et al. Extracellular vesicle and particle biomarkers define multiple human cancers. <i>Cell</i> 2020;182:1044–61.	954
920		955
921		956
922	51. van Niel G, D'Angelo G, Raposo G. Shedding light on the cell biology of extracellular vesicles. <i>Nat Rev Mol Cell Biol</i> 2018;19:213–28.	957
923		958
924	52. Boelens MC, Wu TJ, Nabet BY, Xu B, Qiu Y, Yoon T, et al. Exosome transfer from stromal to breast cancer cells regulates therapy resistance pathways. <i>Cell</i> 2014;159:499–513.	959
925		960
926		961
927	53. Willms E, Johansson HJ, Mager I, Lee Y, Blomberg KE, Sadik M, et al. Cells release subpopulations of exosomes with distinct molecular and biological properties. <i>Sci Rep</i> 2016;6:22519.	962
928		963
929		964
	54. Zhang H, Freitas D, Kim HS, Fabijanic K, Li Z, Chen H, et al. Identification of distinct nanoparticles and subsets of extracellular vesicles by asymmetric flow field-flow fractionation. <i>Nat Cell Biol</i> 2018;20:332–43.	
	55. Wang X, Zhang L, Li H, Sun WJ, Zhang HH, Lai MD. THBS2 is a potential prognostic biomarker in colorectal cancer. <i>Sci Rep-Uk</i> 2016;6:33366.	
	56. Weng TY, Wang CY, Hung YH, Chen WC, Chen YL, Lai MD. Differential expression pattern of THBS1 and THBS2 in lung cancer: clinical outcome and a systematic-analysis of microarray databases. <i>PLoS One</i> 2016;11:e0161007.	
	57. Kashihara H, Shimada M, Yoshikawa K, Higashijima J, Tokunaga T, Nishi M, et al. Correlation between thrombospondin-1 expression in non-cancer tissue and gastric carcinogenesis. <i>Anticancer Res</i> 2017;37:3547–52.	
	58. Zhang H, Deng T, Liu R, Ning T, Yang H, Liu D, et al. CAF secreted miR-522 suppresses ferroptosis and promotes acquired chemo-resistance in gastric cancer. <i>Mol Cancer</i> 2020;19:43.	
	59. Hu YB, Yan C, Mu L, Mi YL, Zhao H, Hu H, et al. Exosomal Wnt-induced dedifferentiation of colorectal cancer cells contributes to chemotherapy resistance. <i>Oncogene</i> 2019;38:1951–65.	
	60. Gunturu KS, Woo Y, Beaubier N, Remotti HE, Saif MW. Gastric cancer and trastuzumab: first biologic therapy in gastric cancer. <i>Ther Adv Med Oncol</i> 2013;5:143–51.	
	61. Yuza K, Nagahashi M, Watanabe S, Takabe K, Wakai T. Hypermutation and microsatellite instability in gastrointestinal cancers. <i>Oncotarget</i> 2017;8:112103–15.	
	62. Uemura N, Okamoto S, Yamamoto S, Matsumura N, Yamaguchi S, Yamakido M, et al. Helicobacter pylori infection and the development of gastric cancer. <i>N Engl J Med</i> 2001;345:784–9.	
	63. Zhao Y, Zhang J, Cheng ASL, Yu J, To KF, Kang W. Gastric cancer: genome damaged by bugs. <i>Oncogene</i> 2020;39:3427–42.	
	64. Keller G, Grimm V, Vogelsang H, Bischoff P, Mueller J, Siewert JR, et al. Analysis for microsatellite instability and mutations of the DNA mismatch repair gene hMLH1 in familial gastric cancer. <i>Int J Cancer</i> 1996;68:571–6.	
	65. Richards FM, McKee SA, Rajpar MH, Cole TR, Evans DG, Jankowski JA, et al. Germline E-cadherin gene (CDH1) mutations predispose to familial gastric cancer and colorectal cancer. <i>Hum Mol Genet</i> 1999;8:607–10.	